

Evaluation of site effects on ground motions based on equivalent linear site response analysis and liquefaction potential in Chennai, south India

Subhadra Nampally · Simanchal Padhy · S. Trupti · P. Prabhakar Prasad · T. Seshunarayana

Received: 26 July 2016 / Accepted: 2 May 2018 / Published online: 15 May 2018
© Springer Science+Business Media B.V., part of Springer Nature 2018

Abstract We study local site effects with detailed geotechnical and geophysical site characterization to evaluate the site-specific seismic hazard for the seismic microzonation of the Chennai city in South India. A Maximum Credible Earthquake (MCE) of magnitude 6.0 is considered based on the available seismotectonic and geological information of the study area. We synthesized strong ground motion records for this target event using stochastic finite-fault technique, based on a dynamic corner frequency approach, at different sites in the city, with the model parameters for the source, site, and path (attenuation) most appropriately selected for this region. We tested the influence of several model parameters on the characteristics of ground motion through simulations and found that stress drop largely influences both the amplitude and frequency of ground motion. To minimize its influence, we estimated stress drop after finite bandwidth correction, as expected from an M6 earthquake in Indian peninsula shield for accurately predicting the level of ground motion. Estimates of shear wave velocity averaged over the top 30 m of soil (V_{S30}) are obtained from multichannel analysis of surface wave (MASW) at 210 sites at depths of 30 to 60 m below the ground surface. Using these V_{S30} values, along with the available geotechnical information and synthetic ground motion database obtained, equivalent linear one-dimensional site response analysis that

approximates the nonlinear soil behavior within the linear analysis framework was performed using the computer program SHAKE2000. Fundamental natural frequency, Peak Ground Acceleration (PGA) at surface and rock levels, response spectrum at surface level for different damping coefficients, and amplification factors are presented at different sites of the city. Liquefaction study was done based on the V_{S30} and PGA values obtained. The major findings suggest show that the northeast part of the city is characterized by (i) low V_{S30} values (<200 m/s) associated with alluvial deposits, (ii) relatively high PGA value, at the surface, of about 0.24 g, and (iii) factor of safety and liquefaction below unity at three sites (no. 12, no. 37, and no. 70). Thus, this part of the city is expected to experience damage for the expected M6 target event.

Keywords South India · MASW · Response spectrum · Site response · Strong ground motion · Liquefaction · PGA

1 Introduction

The Chennai city is situated along the coastal area of Bay of Bengal, mostly consisting of thick layers of soft clay and sand, with recent alluvial material (Fig. 1). The Bureau of Indian Standard upgraded the seismic status of the city from low seismic hazard (zone II) to moderate hazard (zone III) (BIS: 1893 (2001)), meaning that the estimated seismic hazard of the region has been increased from the occurrence earthquakes of moderate

S. Nampally · S. Padhy (✉) · S. Trupti · P. Prabhakar Prasad · T. Seshunarayana
CSIR-National Geophysical Research Institute, Uppal Road, Hyderabad 500007, India
e-mail: spadhy@ngri.res.in

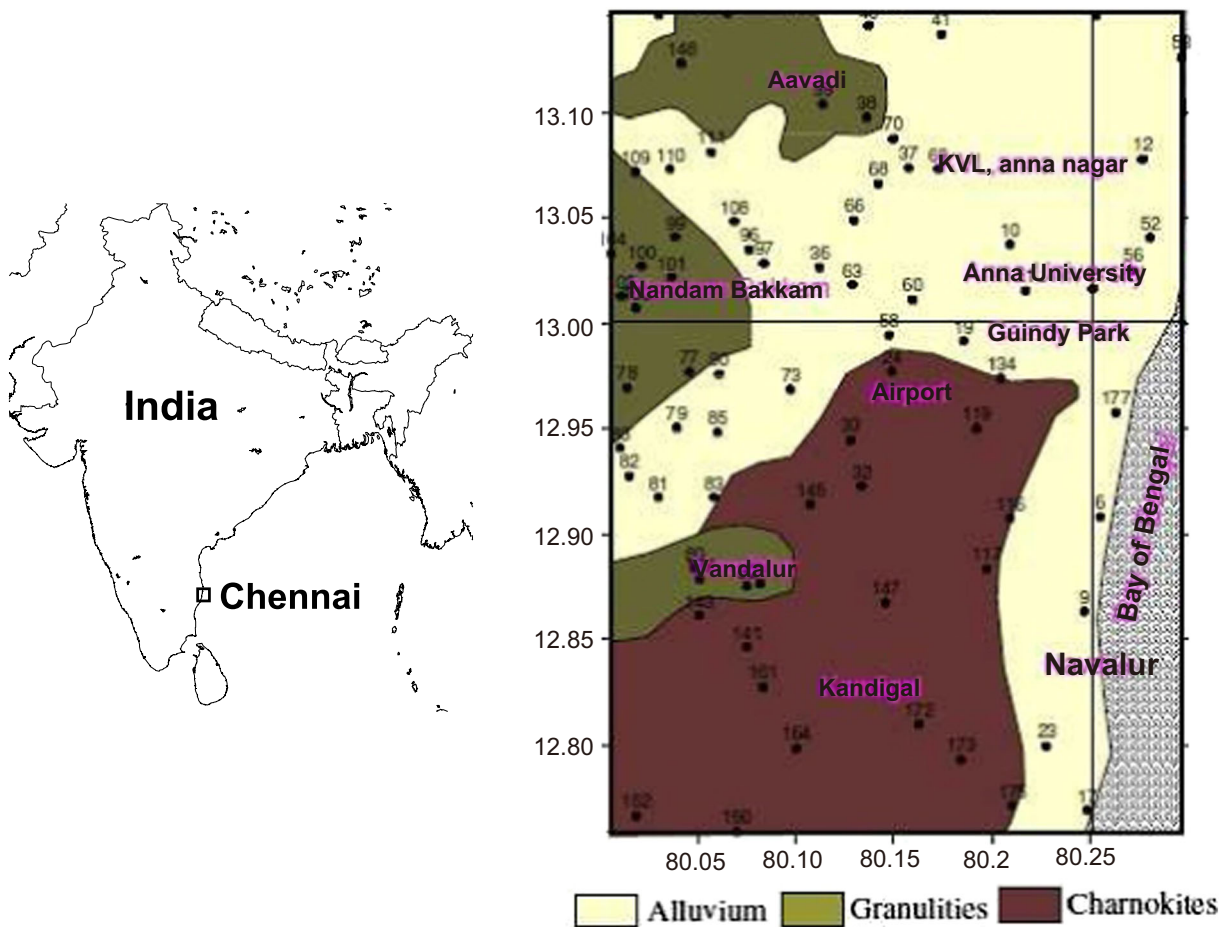


Fig. 1 Map of India showing the location of the Chennai city located in south India, as marked by a small rectangle. The study area over the city is enlarged showing the detailed geology of different parts of the city

magnitudes in the historical past to the occurrence of earthquakes with magnitude greater than or equal to 5.0 in 18th century (Ganapathy 2005). Occurrence of large earthquakes in the vicinity of the city may cause extensive damage to the built environment, due to either amplified ground motions or liquefaction of soft sediments. Therefore, a better understanding of the relationship between soft sediments and damage pattern due to seismically induced ground motion amplification and soil liquefaction is a basic step towards seismic hazard assessment in the city. Preliminary seismic hazard assessment of Chennai city was carried out by Boominathan et al. (2008), who adopted the equivalent linear method of one-dimensional ground response analysis for estimating the ground motion parameters at several sites in the city. They found significant site amplification due to the deep soil

sites with clayey or sandy deposits in the central and southern parts of the city. Ganapathy (2011) developed a first-level seismic microzonation map of Chennai in the Geographical Information System (GIS) platform by integrating the five thematic maps of weighted values of PGA, velocity of S-waves at 3 m, geology, groundwater fluctuations, and bedrock depth. Furthermore, he used the ground motion attenuation relationship of Iyengar and Ragukanth 2004 and obtained the average V_s in the depth interval 0–3 m using the empirical relations of Imai and Yoshimura (1970) and Ohba and Goto (1978).

In this study, we developed a spatial distribution of site-specific strong ground motion amplification and liquefaction potential for the Chennai city. We conducted a multichannel analysis of surface wave (MASW) survey within the city and obtained

average shear wave velocity at each site down to 30–60-m depth below the surface. We then performed an equivalent linear analysis in SHAKE2000 using the ground motion from EXSIM as the input motion to estimate PGA at the soil surface, amplification ratio (PGA at the soil surface/PGA of the input ground motion) for different sites in the city. Synthetic ground motion records were calculated for the maximum credible earthquake of M6, assuming the Palar fault as the source for this event (Fig. 2). We used the modified stochastic finite-fault technique based on the dynamic corner frequency approach (Motazedian and Atkinson 2005) to synthesize the acceleration time history. The one-dimensional site response analysis was carried out for its simplicity using the SHAKE2000 program (Ordóñez 2003) for characterizing the 210 sites in the depth range 30–60 m below ground level. If the shear strains are less than 0.05%, then equivalent linear analysis can be used for evaluation of site response. For large shear strains, however, any nonlinear analysis program like DEEPSOIL (Hashash et al. 2011), DMOD (Matasovic 1993), or DESRA (Lee and Finn 1978) can be used for a more realistic modeling of nonlinear soil response (Kaklamanos et al. 2015; Carlton and Tokimatsu 2016). We mapped the fundamental frequency, amplification, and factor of safety (FS) against liquefaction for each site in the city based on the cyclic stress approach of Seed and Idriss (1971).

2 Geology and tectonic setting of the area

The geology of Chennai mainly includes the Archaean crystalline rocks, Gondwana and Tertiary sediments, and recent alluvium (Ganapathy and Rajawat 2014). The alluvium dominates the city comprising of clays, sands, sandy clays, and occasional boulder or gravel zones. The coastal region of the city is filled with marine sediments containing clay-silt sands (Maheswari et al. 2010). Igneous or metamorphic rocks are found in the southern parts, marine sediments are found in the eastern and northern parts, and alluvium and sedimentary rocks are found in the western parts of the city (Fig. 1) (Ganapathy and Rajawat 2014).

The crystalline basement ridge separates the city into two basins: the southern basin that shallows without

Gondwana sediments and the northern basin with extensive sediments beneath the alluvium. The NW-SE trending Chennai Nasik Lineament (CNL) runs from the east coast to north of Mumbai, is close to Surat on the west coast, and extends further towards NW into the Saurashtra Peninsula. The 1993 Latur earthquake in Peninsular India occurred close to the CNL. The uplift of Eastern Ghats Physiographic Province is well illustrated by a change in the courses of rivers, such as Pennar, Palar (Paleo delta north of Chennai and at present south of Chennai), and Cauvery (Radhakrishna 1992). Nellore Khammam Schist Belt and Eastern Ghat Granulite Belt were uplifted because of anticlockwise rotation of East Coast Sedimentary Basin (ECSB). The subducted oceanic crust of the Bay of Bengal towards Burma develops the East Coast Sedimentary Basins and neo-tectonism and seismic activity in the eastern part of South India and Bay of Bengal (Rao and Babu 1995).

3 Methodology

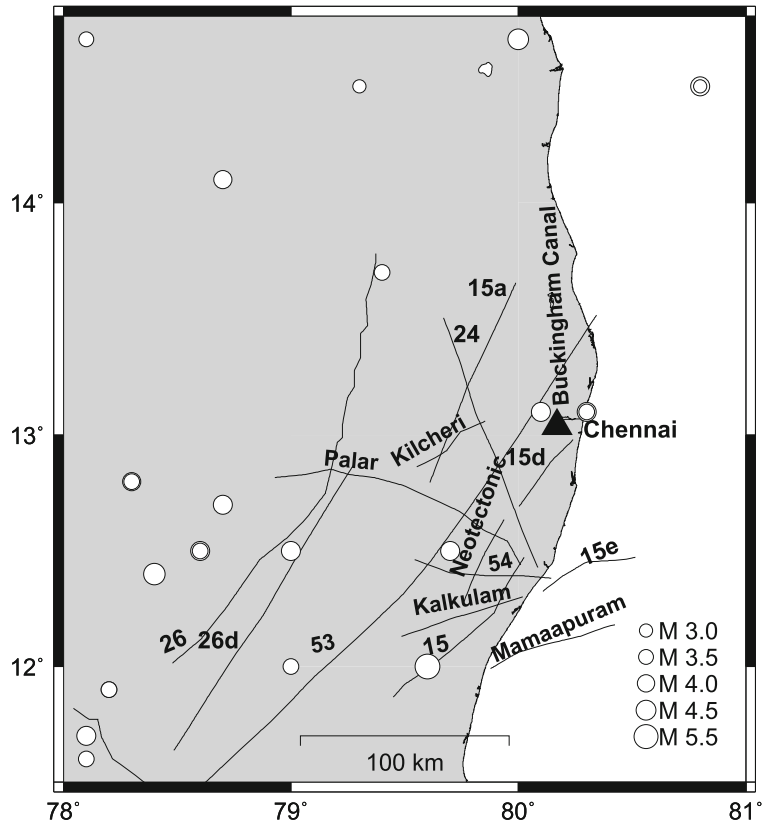
3.1 Finite-fault modeling of strong ground motion records

The stochastic finite-fault method, based on dynamic corner frequency approach of (Motazedian and Atkinson 2005), was used to simulate strong ground motion records. In this method, the entire fault plane is divided into small sub-faults. Each sub-fault represents a point source characterized by a ω^2 source model (Brune 1970). The ground motion due to the entire fault, $a(t)$, can then be obtained by summing the motion due to each sub-fault, $a_{ij}(t)$, calculated based on the stochastic point source method (Boore 1983), with a proper time delay as (Motazedian and Atkinson 2005):

$$a(t) = \sum_{i=1}^{nl} \sum_{j=1}^{nw} H_{ij} \times a_{ij}(t - \Delta t_{ij}), \quad (1)$$

where nl and nw are the number of sub-faults along the length and width of the large fault, respectively, $N = nl \times nw$ is the total number of sub-faults, Δt_{ij} is the relative time delay for the energy radiated from the ij^{th} sub-fault to reach the observation point, and H_{ij} is a normalization factor for the ij^{th} sub-fault that scales the source spectrum in order to conserve total radiated energy of sub-faults at high frequencies. The scaling factor H_{ij} is given as (Motazedian and Atkinson 2005):

Fig. 2 Map of the relatively larger area of south India showing the location of the Chennai city (triangle), earthquakes with magnitudes greater than 3 in the region taken from the USGS catalog (circles), target event of M6 (star) located on the Palar fault, and the seismotectonic features (lines). The filled circles with numerals represent the locations of the sites where geophysical studies are carried out. The numerals represent different tectonic features over the study area (modified after Boominathan et al. 2008)



$$H_{ij} = \left(\frac{N \sum_f \left(\frac{f^2}{1+(f/f_0)^2} \right)^2}{\sum_f \left(\frac{f^2}{1+(f/f_{0ij})^2} \right)^2} \right)^{1/2}, \tag{2}$$

where f_0 and f_{0ij} are the corner frequency of the entire fault and dynamic corner frequency of the ij^{th} sub-fault, respectively. The lower limit of f_{0ij} is the corner frequency of the entire fault, f_0 . The frequency, f_{0ij} , can be defined in terms of the cumulative number of sub-faults ruptured at time t , $N_R(t)$ as:

$$f_{0ij} = 4.9 \times 10^6 \left(N_R(t)^{-1/3} \right) N^{1/3} \beta \left(\frac{\Delta\sigma}{M_0} \right)^{1/3}, \tag{3}$$

where β is shear wave velocity (km/s), M_0 is seismic moment (N m), and $\Delta\sigma$ is stress drop (bar). The use of dynamic corner frequency helps in obtaining the resultant acceleration spectrum with energy over a wide frequency range, independent of size of sub-fault. The use of both dynamic corner frequency and scaling source spectrum based on the scaling factor, H_{ij} , produces constant level of the resulting acceleration

spectrum, independent of number and size of sub-faults. The acceleration spectrum of the ij^{th} sub-fault, based on the Brune source model, can be expressed as (Boore 1983):

$$A_{ij}(f) = CM_{0ij} \frac{(2\pi f)^2}{\left(1 + \left(\frac{f}{f_{0ij}(t)} \right)^2 \right)} \left\{ \frac{\exp\left(-\frac{\pi f R_{ij}}{\beta Q(f)} \right) \exp(-\pi f \kappa)}{R_{ij}} \right\}, \tag{4}$$

where $C = \frac{R_{\theta\varphi} F V}{\rho \pi \beta^3}$ is a constant, $R_{\theta\varphi}$ is the radiation pattern (average value of 0.55), ρ is the density (2.8 g/cm³), β is the S-wave velocity (3.5 km/s), F is the free surface amplification (2.0), V (=0.71) is the partition of S-wave energy into two horizontal components, M_{0ij} is the seismic moment of the ij^{th} sub-fault, $Q(f)$ is the frequency-dependent quality factor, κ is near-surface attenuation that explains the decay of acceleration at high frequencies (Anderson and Hough 1984), and f_{0ij} is the dynamic corner frequency of the ij^{th} sub-fault, that is function of time, t . The seismic moment of each sub-fault is given by $M_{0ij} = M_0/N$, where M_0 is the moment

of the entire fault and N represents the total number of sub-faults.

Using this theory, we synthesized strong ground motion records with the appropriately selected parameters characterizing the source (rupture dimension, fault orientation, stress drop, etc.), propagation path (shear wave velocity, density, attenuation parameter, geometrical spreading, etc.), and site (near-surface attenuation, site amplification, etc.) discussed as follows. Based on the available seismo-tectonics of the area, the nearest active fault was chosen as the Palar fault (Fig. 2). We considered the event location (12.60° N, 79.82° E) on the Palar fault. We have chosen $M = 6$ as the MCE based on the seismicity associated with the Palar fault, which is at ~ 50 km away from the city. The model parameters for the synthesis of ground motion for this target event (M6) are listed in Table 1. The rupture dimensions were estimated using the source scaling relationship of Wells and Coppersmith (1994) for this magnitude. The relation $Q = 800f^{0.42}$, obtained for the Indian Shield region (Singh et al. 2004), was used to characterize the frequency-dependent attenuation of the medium. A kappa value of $\kappa \sim 0.035$ s was used to characterize the near-surface attenuation for the site.

3.2 Measurement of shear wave velocity

Park et al. (1999a, b) proposed the MASW method to determine the near-surface velocity structure. Here, the Rayleigh wave dispersion curves are inverted to obtain the S-wave velocity of the upper 30 m of soil column (V_{S30}). In this technique, Rayleigh waves are recorded by multiple receivers at finite distances from the source. The details of the technique can be found in its recent application by the authors for studying microzonation of the Nanded city in western India (Subhadra et al. 2015).

The MASW test was carried out at 210 sites in the study area. The parameters, such as the distance of source to the first and last receiver, and the spread length of survey lines were selected based on the signal-to-noise ratio (SNR) and the depth (more than 30 m) of investigation. The values of V_{S30} obtained for the selected sites in the city are in the range 100–1500 m/s.

3.3 One-dimensional ground response analysis

Ground response analysis in one-dimensional refers to the response of soil layers to vertically incident SH-waves from the underlying rock formation, which was

Table 1 Modeling parameters for an expected earthquake of magnitude 6.0 in Chennai city

Earthquake magnitude	6.0
Latitude, longitude	12.60° N, 79.82° E, USGS
Hypocenter depth (km)	10
Fault strike°, dip°	102°, 50°
Fault length (km), width (km)	2.5, 2.5, Wells and Coppersmith (1994)
Shear wave velocity (km/s)	3.5
Crustal density (g/cm ³)	2.8
Stress drop (bars)	200
Near-surface attenuation, Kappa	0.035
Anelastic attenuation $Q(f)$	$800f^{0.42}$, Singh et al. (2004)
Geometrical spreading R^b ; $b =$	$1/R$ ($R \leq 40$ km) $1/R^{0.5}$ ($40 \leq R \leq 80$ km) $1/R^{0.55}$ ($R \geq 80$ km), Bodin et al. (2004)
Duration	(0–10 km) + 0.16 (10–70 km) – 0.03 (70–130 km) + 0.04 (> 130 km), Atkinson and Boore (1995)
Crustal amplification	B/C boundary, Atkinson and Boore (2006)
Windowing function	Saragoni-Hart
Pulsing area	50%, Motazedian and Atkinson (2005)

conducted using the program SHAKE2000 (Ordóñez 2003). SHAKE2000 assumes a model consisting of horizontally extended, homogeneously, and isotropically distributed soil layers above the half-space and relatively flat underlying bedrock interface. Each soil layer is assumed to be homogeneous and isotropic, that is characterized by its thickness (m), shear wave velocity (m/s) in the layer, total unit weight (kN/m³), damping (%), maximum shear stress (kN/m²), and maximum shear strain (%). The model assumes half-space as the rock formation underlying a soil deposit, and the half-space lies at the depth of bedrock. Thus, the transfer function between the half-space and the free surface is convolved with the input motion defined at the bedrock to compute the motion at the free surface. Nonlinearity of soil profiles, expressed in terms of shear modulus, modulus reduction, and damping ratio, is considered by the use of equivalent linear analysis performed with an iterative technique (Idriss and Seed 1968; Seed and Idriss 1970). With this technique, linear analyses with

the soil properties are performed and are iteratively adjusted to be consistent with an effective level of shear strain induced in the soil. We used $G_{\max} = 20.885$ ksf and damping ratio = 0.05% for the equivalent linear soil response analysis for the elastic base. We used the shear modulus reduction and damping curves based on local geology of the Chennai city (Boominathan et al. 2008; Maheswari et al. 2010; Ganapathy and Rajawat 2014). Included G/G_{\max} curves are (1) sand S1 (CP < 1.0 KSC, Sun et al. 1988), (2) clay C3 (PI 20–40, Sun et al. 1988), (3) gravel average (Seed et al. 1986), and (4) rock (Schnabel 1973). Similarly, damping curves which are included here are (1) sand (Seed and Idriss 1970), (2) clay (Seed and Idriss 1970), (3) gravel average (Seed et al. 1986), and (4) rock (Schnabel 1973). Tables 2 and 3 list the soil profile (V_s and unit weight with depth for specific layers) used for the equivalent linear analysis for site no. 67 and no. 175.

3.4 Evaluation of liquefaction potential

The liquefaction hazard in Chennai was assessed in terms of FS. Evaluation of liquefaction potential, based on the cyclic stress approach, involves comparison of the level of cyclic stress induced by the earthquake (loading) with the level of cyclic stress required to initiate liquefaction (resistance). Liquefaction can be expected at depths where the loading exceeds the resistance, the soil is susceptible to liquefaction (i.e., a sandy soil), and the soil is saturated. The liquefaction potential can generally be quantified in terms of FS against

Table 2 The soil profile used in the equivalent linear soil response analysis for the site no. 67

Soil layer	Depth (m)	V_s (m/s)	Unit weight (kN/m ³)
1	1.10	216.32	15
2	2.49	275.65	15
3	4.22	294.32	16
4	6.38	180.24	16
5	9.09	158.37	16
6	12.47	231.46	17
7	16.69	296.36	17
8	21.98	300.12	18
9	28.58	262.19	18
10	35.72	382.89	19

Table 3 The soil profile used in the equivalent linear soil response analysis for the site no. 175

Soil layer	Depth (m)	V_s (m/s)	Unit weight (kN/m ³)
1	3.22	2761.68	19
2	7.25	2830.14	19
3	12.32	2883.62	19
4	18.58	2863.40	19
5	26.46	3170.33	20
6	36.3	3587.00	21
7	48.59	3431.17	21
8	63.97	3269.4	20
9	83.19	2933.28	21
10	103.98	4100	22

liquefaction and it is defined as (Idriss and Boulanger 2006):

$$FS = \frac{CRR}{CSR}, \quad (5)$$

where the cyclic resistance ratio (CRR) and cyclic stress ratio (CSR) are the resistance to liquefaction and the earthquake-induced loading, respectively. The ratios CSR and CRR being function of depth, the liquefaction potential is evaluated at corresponding depths within the soil profile. Liquefaction is predicted to occur when $FS < 1$ and not to occur when $FS > 1$. FS of a soil layer can be calculated with the help of several tests, such as the Standard Penetration Test (SPT), Cone Penetration Test (CPT), Becker Penetration Test (BPT), and shear wave velocity (V_s) test (Youd et al. 2001).

3.4.1 Cyclic stress ratio

CSR characterizes the earthquake-induced seismic loading that can be determined from PGA estimated from the site-specific strong ground motion records. In cyclic stress approach, the excess pore pressure and hence seismic loading are related to the earthquake-induced cyclic shear stress. Evaluation of liquefaction potential and hence excess pore pressure to initiate liquefaction depends on the amplitude and number of cycles (or duration) of earthquake-induced shear stress. Because the duration of ground motion varies with the magnitude of earthquake, the CSR also varies with the size of the

earthquake. The magnitude-corrected CSR at depth z (m) can be expressed (Seed and Idriss 1971; Goda et al. 2011) as:

$$CSR = 0.65 \frac{PGA}{g} \frac{\sigma_v}{\sigma_v^0} \frac{r_d(z)}{MSF(M)}, \tag{6}$$

where 0.65 is a weighting factor to account for the equivalent series of uniform stress cycle, that is normally taken at 65% of the maximum shear stress, g is the acceleration of gravity; σ_v and σ_v^0 are the total vertical overburden stress and effective vertical overburden stress, respectively, at a given depth below the ground surface; r_d is depth-dependent stress reduction factor that accounts for the dynamic response of the soil column and represents the variation of shear stress with depth; and MSF is the magnitude scaling factor that is a function of magnitude of earthquake, M . The stress reduction factor, r_d , can be expressed as (Idriss and Boulanger 2006):

$$r_d = \exp[\alpha(z) + \beta(z)M_w], \tag{7}$$

where $\alpha(z)$

$$= -1.012 - 1.126 \sin\left(\frac{z}{11.73} + 5.133\right), \text{ and} \tag{8}$$

$$\beta(z) = 0.106 + 0.118 \sin\left(\frac{z}{11.28} + 5.142\right), \tag{9}$$

The factor MSF is calculated using the formula proposed by Idriss (1999) as:

$$MSF = 6.9 \exp\left(\frac{-M_w}{4} - 0.06\right) \text{ for } M_w > 5.2 \tag{10}$$

where M_w is the moment magnitude of the earthquake.

3.4.2 Cyclic resistance ratio

CRR is a measure for evaluation of liquefaction resistance (capacity of soil to resist liquefaction). The methods used for the evaluation of CRR employ lab testing of undisturbed in situ soil specimens retrieved with drilling and sampling techniques. To avoid the difficulties associated with lab testing, especially for retrieving soil specimens, several field tests have become popular for evaluation of liquefaction resistance. Of several tests, the shear wave velocity, V_S -based

technique for characterizing liquefaction resistance is widely used because of its nondestructive and nonintrusive features, where a shear wave velocity profile can be established using surface wave velocity measuring techniques without the need of drilling and penetration.

One important factor influencing the dynamic properties of soil is the shear wave velocity, V_S , corrected for the state of stress in soil (Hardin and Drnevich 1972). The results from laboratory test show that the velocity of a propagating shear wave depends on principal stress in the direction of wave propagation (Roesler 1979; Stokoe and Nazarian 1985; Belloti et al. 1996). Here, V_S is corrected for overburden stress using the following relation (Robertson et al. 1992):

$$V_{S1} = V_S C_V = V_S \left(\frac{P_a}{\sigma_v'}\right)^{0.25}, \tag{11}$$

where V_{S1} is the overburden stress-corrected shear wave velocity; C_V is the factor used to correct the measured shear wave velocity for overburden pressure, P_a is the reference stress of 100 kPa or about 1 atmospheric pressure, and σ_v' is the initial effective overburden stress in kilopascal. A maximum value of $C_V = 1.4$ is generally applied to the V_S data at shallow depths.

Next, CRR can be evaluated from V_{S1} following the Andrus and Stokoe's (2000) curve obtained, based on an expanded database that includes 26 earthquakes and more than 70 measurement sites, as:

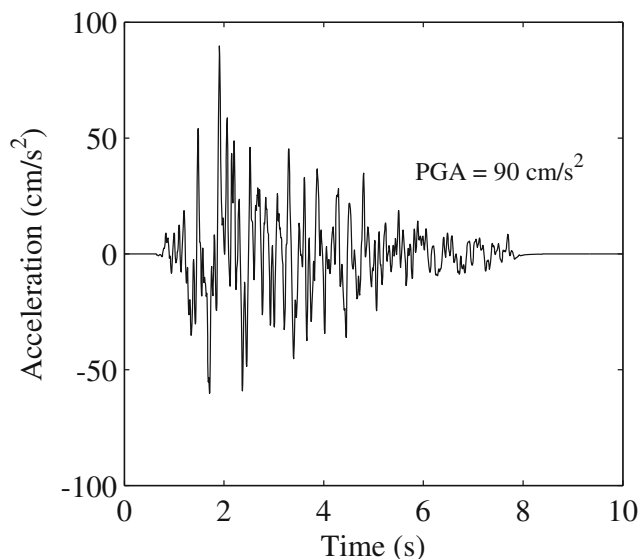
$$CRR = 0.022 \left(\frac{V_{S1}}{100}\right)^2 + 2.8 \left[\frac{1}{(V_{S1}^* - V_{S1})} - \frac{1}{V_{S1}^*} \right], \tag{12}$$

where V_{S1}^* is the upper limit of V_{S1} for occurrence of liquefaction in soils (V_{S1}^* linearly varies from 200 to 215 m/s for fines content between 35 and 5%).

4 Results and discussion

Figure 3 shows an example of synthetic strong ground motion record derived from the finite-fault model for an earthquake of magnitude M6 at a rock site no. 150, SW of the Chennai city, located at a distance of 35 km from the source. The effect of site can be described in terms of parameters such as the near-surface attenuation and site

Fig. 3 Synthetic ground motion obtained for the M6.0 target event using the model parameters listed in Table 1 and for a source-receiver distance of 35 km from the Palar fault as the source. A PGA of 90 cm/s^2 is shown



amplification (see Table 1). In general, parameters such as near-surface attenuation, κ , anelastic attenuation, Q^{-1} , stress drop, $\Delta\sigma$, and source mechanism influence the characteristics (amplitude and duration) of ground motion synthesized. The influence of κ , Q , and $\Delta\sigma$ on both amplitude and duration of synthetic ground motion records as well as on their Fourier amplitude spectrum (FAS) are shown in Fig. 4A–C. The amplitude of ground motion becomes lower with an increase in κ (increased near-surface attenuation, Fig. 4A), decrease in Q (increase in attenuation, Fig. 4B), and lowering in $\Delta\sigma$ (Fig. 4C). The influence of Q (Fig. 4B) and stress drop (Fig. 4C) is more than that of κ (Fig. 4A) on ground motion amplitude. As expected, the response spectra decay faster at high frequencies ($> \sim 5 \text{ Hz}$) for higher values of κ (Fig. 4a–f). The events with high stress drop value radiate more high frequency energy than the events with low stress drop value. Similarly, the spectra decay faster at high frequencies for lower values of Q (higher attenuation) (Fig. 4B), that agrees with the fact that high frequency energy decay faster in a medium with high attenuation (low Q). In regard to stress drop, the maximum amplitude of FAS is found to be more for high stress drop values than that for low stress drops, although their effect on the FAS seems to be small (Fig. 4b–d, f). Stress drop is an important parameter controlling the characteristics of ground motion and its spectrum. Its value was appropriately chosen from an earthquake of similar magnitude in the area. Because finite bandwidth is found to underestimate the values of

stress drop (Padhy and Subhadra 2016), its value was used after it is corrected for the finite bandwidth effect for accurately modeling the ground motion records. We used the relationship between estimated and true value of stress drop obtained for the Brune circular source model (Di Bona and Rovelli 1988) to correct the estimates of stress drop to obtain the true estimates.

The finite-fault method of strong-motion simulation described by Motazedian and Atkinson (2005) considers an extended source based on dynamic corner frequency approach. Their approach had a significant advantage over previous methods in that the simulation results are insensitive to sub-source size. In order to see how well the finite-fault source geometry controls the ground motion characteristics, we analyzed synthetic ground motion records taking into account the finite-fault geometry expressed by strike and dip of fault plane of large earthquakes that occurred in peninsular shield of India. We found high PGA value for events characterized by the thrust mechanism of the 1993 Latur and 2001 Pondicherry earthquakes. The synthetic ground motions obtained for the strike-slip focal mechanisms of the three events that occurred in Peninsular India (the 1967 Ongole, 1969 Bhadrachalam, and 2014 Bay of Bengal earthquakes) exhibit low PGA and longer duration of ground motion records (Fig. 5). In any case, the simulation results obtained here need, however, to be tested against observations to validate the results showing the influence of source radiation on ground motion amplitudes.

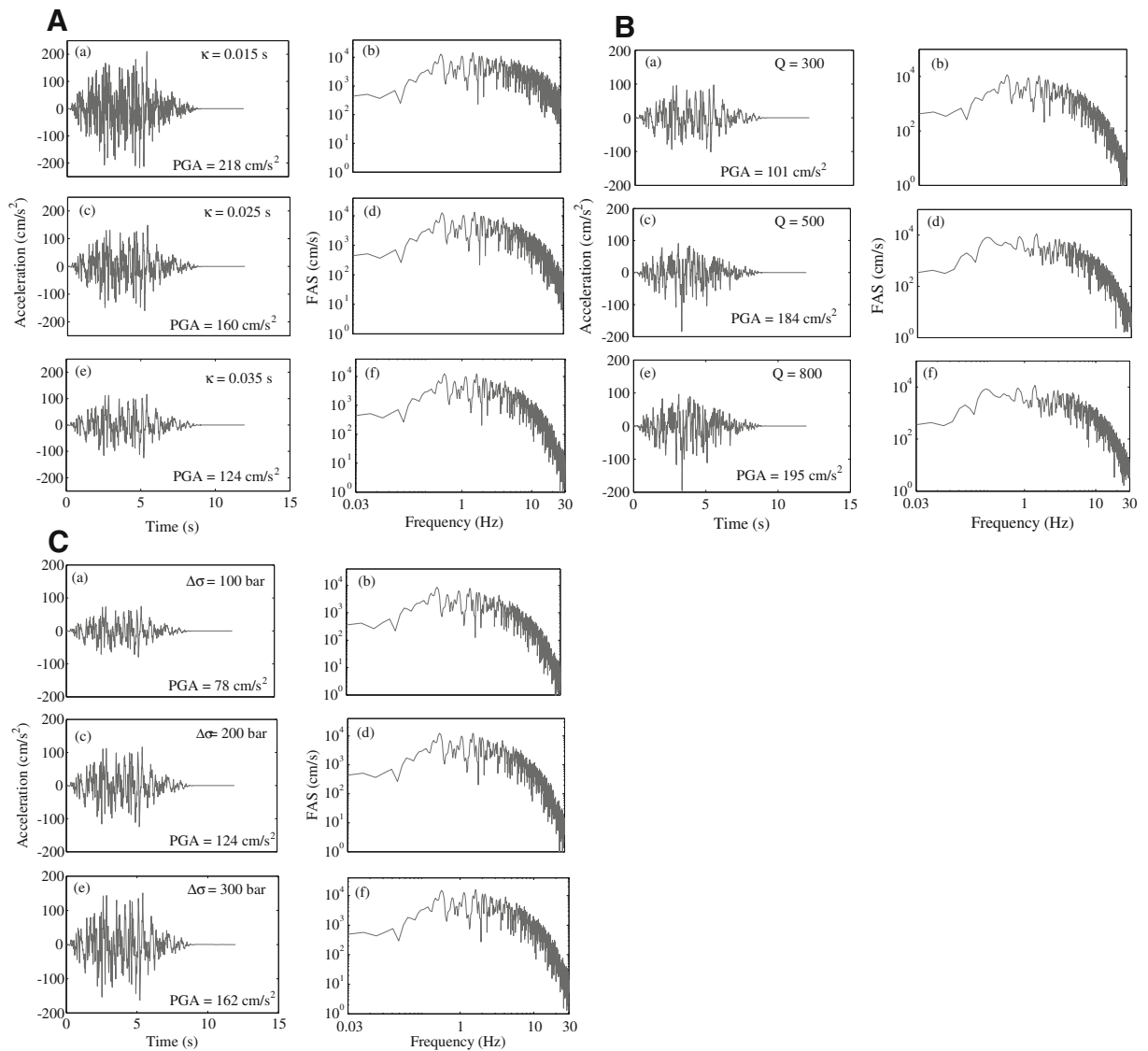


Fig. 4 Effects of **A** near-surface attenuation κ , **B** intrinsic attenuation, Q^{-1} , and **C** stress drop $\Delta\sigma$ on synthetic strong ground motion record. The ground motion records (**a**, **c**, and **e**) and their

corresponding response spectra (**b**, **d**, and **f**) are shown for each case. The values of the corresponding parameters for which the synthetic records were obtained are shown in each frame

Figure 6 shows the V_{S30} distribution over the city that was obtained with a gridding method based on the weighted average interpolation of the V_s values measured with the MASW method. The high V_{S30} values (1400–1500 m/s) are found for the northwest and southern parts of the study area, characterized by Granulites and Charmokites types of rock. The northeast part is characterized by relatively low V_{S30} values (<200 m/s), which may be associated with coastal area of the city carrying alluvial deposits. The depth sections of V_{S30} for both soil and rock sites obtained from MASW are shown

in subpanels a and b of Fig. 7, respectively. The soil profile expressed in terms of unit weight and shear wave velocity at corresponding depths for both the sites is listed in Tables 2 and 3. Relatively low values of V_{S30} (<250 m/s) are observed at top 12-m depth at soil sites (site no. 67, Fig. 7a), while high values of V_{S30} (3200–4800 m/s) are observed at 75-m depth at rock sites, with a strong lateral variation in V_{S30} (site no. 175, Fig. 7b).

The estimated PGA values both at the free surface and at the rock level are now mapped (Fig. 8). The PGA estimates range from 0.11 to 0.24 g at surface (Fig. 8a)

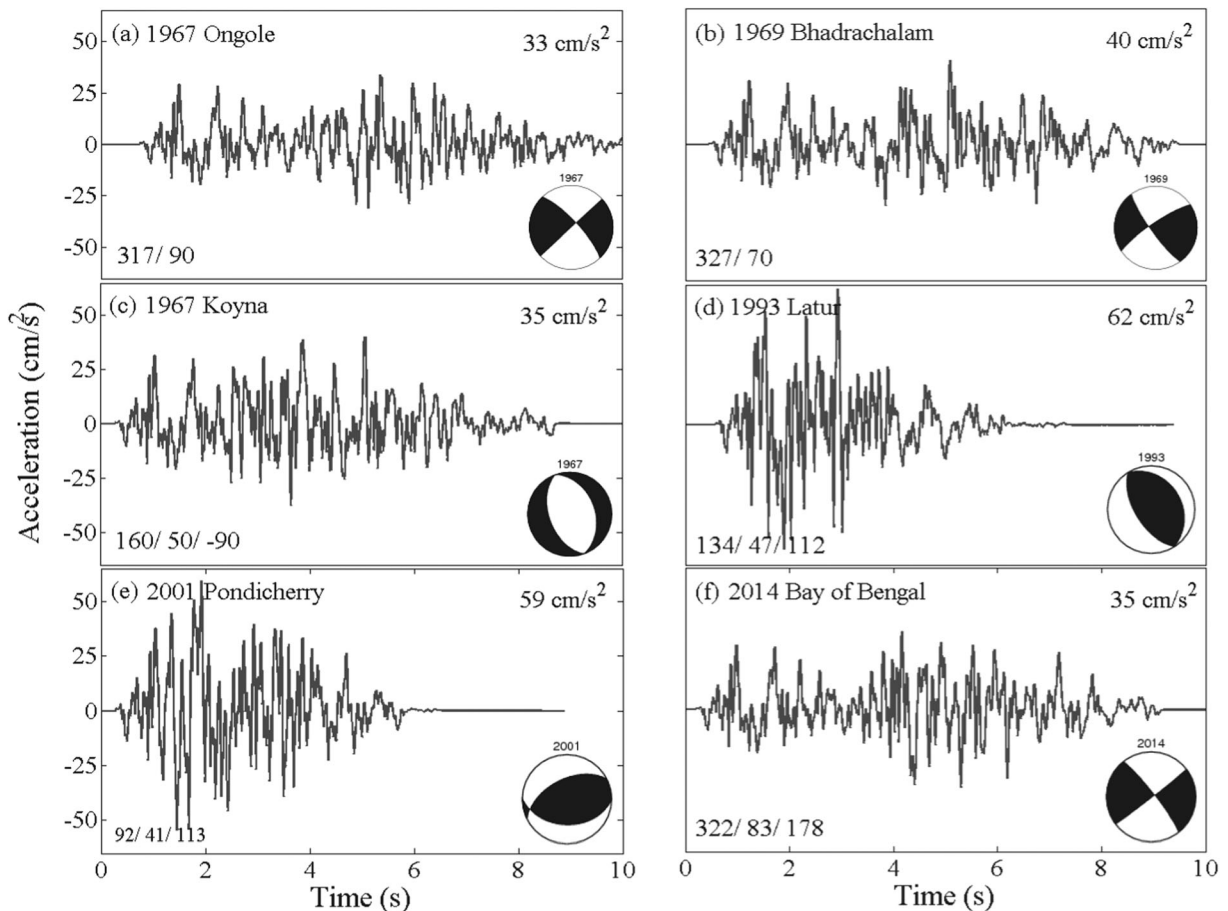


Fig. 5 Effect of focal mechanism on the nature of synthetic strong ground motion records for (a–f) different earthquakes occurred in south India. The values of strike, dip, and rake and the corresponding beach-ball showing the focal mechanism solution are shown

for some earthquakes. The beach balls are not shown for those earthquakes for which any of the parameters like strike/dip/rate is not available. The PGA values obtained from synthetic records are mentioned against each earthquake

and from 0.08 to 0.13 g at rock (Fig. 8b); the depth to rock beneath the area varies from 3 to 21 m (Fig. 8c). According to the NEHRP soil profile, rock is defined in terms of the V_s value greater than 760 m/s. We calculated the ground motion from EXSIM as the input motion for the SHAKE2000 analysis. We modeled only the soil layers in SHAKE2000 to estimate PGA at the soil surface.

The high PGA values observed at ground surface (Fig. 8a) correspond to low shear wave velocities. The northeast part of the city is characterized by relatively high PGA values both at the surface and rock levels. The value of rock level PGA is relatively more on the NE part than on the SE part of the city (Fig. 8b), where the difference in PGA could be related to the regional variation in impedance contrast between surface and underlying deposits (Zhao 2011; Dobry and Iai 2001),

among other details such as the stratigraphy and the material damping. The variation in rock level PGA at ~15-m depth at a coastal area is found to be small (Fig. 8b). The effect of shallow soft layers shows high amplification than the deep soil layers (Fig. 8c).

Figure 9 shows the variation of PGA with depth at site no. 12 for the M6 target event. The PGA value varies from 0.09 to 0.225 g between the surface and 16-m depth. Figure 10 shows the spectrum of the amplification ratio (amplification at 0.145 m to that at 16-m depth) at site no. 12 obtained with a 5% damping, with a peak value found around 4 Hz. Figure 11 shows site-specific response spectra for different damping levels at ground surface for the site no. 12, as an example. It is seen that the spectral accelerations for different damping coefficients exhibit peak around 0.2 s. It is worth to note that the fundamental natural frequency of the site is

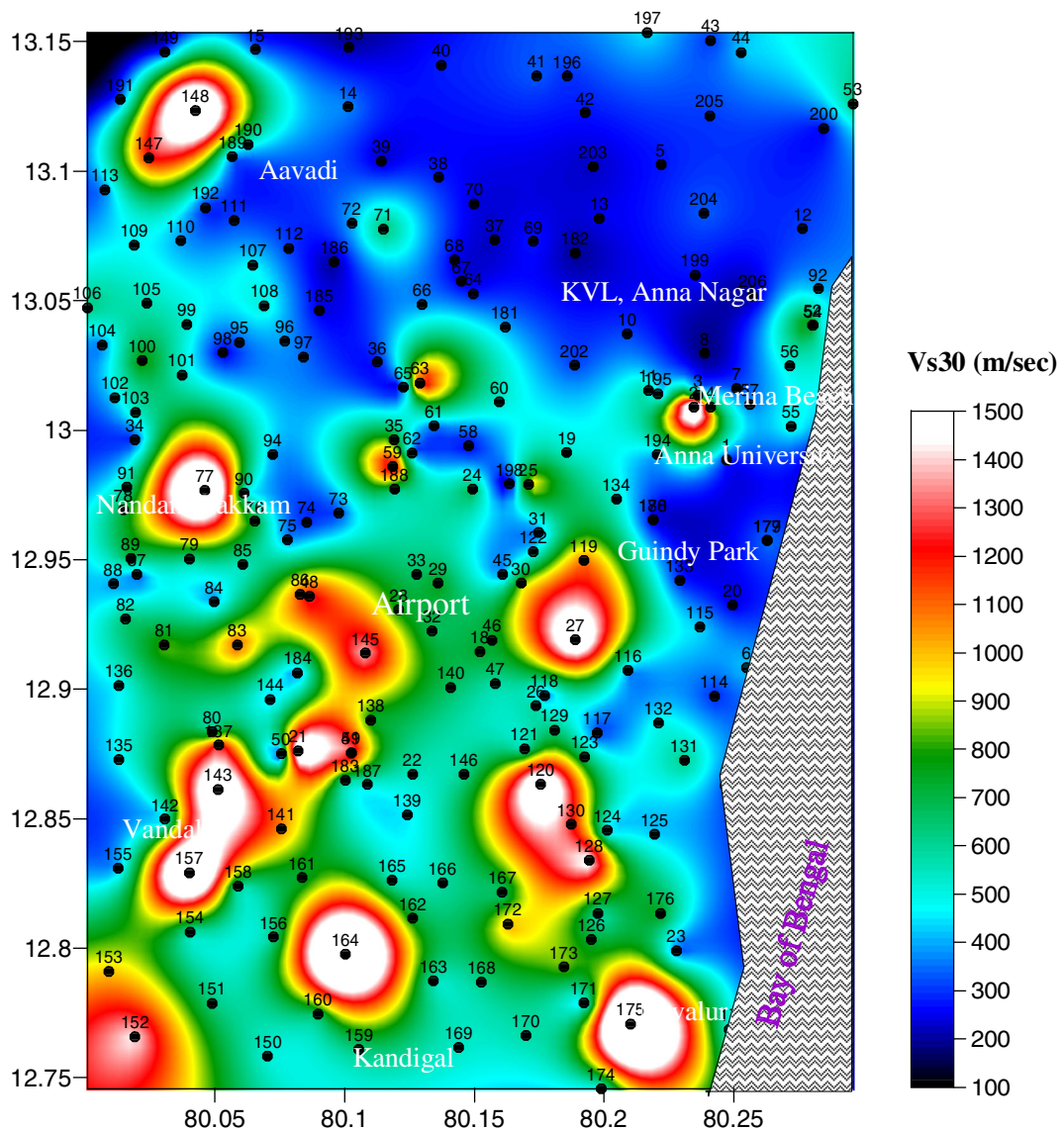


Fig. 6 Map showing the distribution of average shear wave velocity V_{S30} (m/s) for the city obtained with MASW. The MASW testing locations are marked with small circles and site numerals on the map. Note the northeastern part of the area characterized by low V_{S30} values in the range 100–300 m/s

with numerals on the map. Note the northeastern part of the area characterized by low V_{S30} values in the range 100–300 m/s

more important than the predominant frequency of the input ground motion because it does not change (or changes very little), whereas the predominant frequency of the input motion changes with each earthquake and is therefore difficult to predict. We computed the fundamental natural frequency of the site by using the relation $f_0 = V_{S30}/4H$, where H is the soil thickness of the particular site. Figure 12 shows a map of the fundamental natural frequency of the sites analyzed. It is found that the sites in the northern part of the city are characterized by fundamental frequency of < 3 Hz, while most of the

sites in the central and south-to-southwest parts are characterized by fundamental frequency of > 6 Hz. The characteristic site frequencies vary with ground type, ranging from ~ 1 Hz for soft soil sites to ~ 20 Hz for the stiff rock sites (Fig. 12).

The amplification factor is evaluated as the ratio of the PGA at the ground surface to the PGA at the bedrock for different sites based on the SHAKE2000 analysis (Anbazhagan and Sitharam 2008; Subhadra et al. 2015). As already mentioned, we define rock as the depth where the MASW measurements are more than

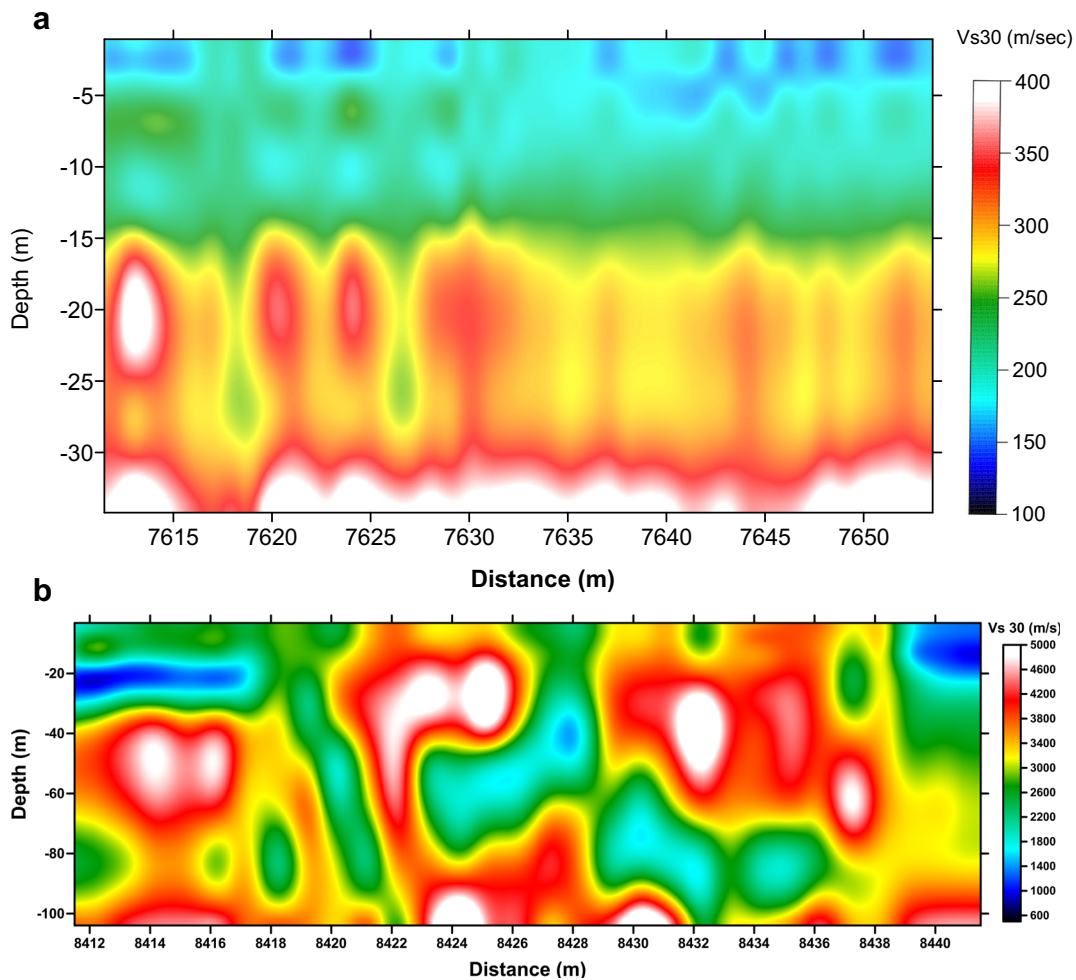


Fig. 7 a Variation of two-dimensional shear wave velocity with depth near the **b** site no. 67 at low velocity zone and **c** site no. 175 at high velocity zone

760 m/s, which is also the depth of half-space and input ground motion used in the SHAKE2000 analyses. The amplification map of the city (Fig. 13), obtained by mapping of the amplification factor, ranged from 2 to 7.5 for the M6 target event. Figure 13 shows that some sites in the northeast part of the city are characterized by high amplification factor in the range 6.0–7.5 at ~ 4 Hz (Fig. 10) and the V_{S30} values in the range 200–400 m/s (Fig. 6). This zone can be considered as a significant zone of ground motion amplification. Sites with high amplification factors indicate higher seismic potential and hence are more prone to high seismic hazard. Based on the range in V_{S30} and the corresponding site amplification factor, we propose that the city can be divided into five zones (Table 4): zone I ($V_{S30} = 750$ –1500 m/s, Amp. Factor = 3.0–3.99), zone II ($V_{S30} = 450$ –750 m/s,

Amp. Factor = 4.0–4.99), zone III ($V_{S30} = 350$ –450 m/s, Amp. Factor = 5.0–5.99), zone IV ($V_{S30} = 200$ –350 m/s, Amp. Factor = 6.0–6.99), and zone V ($V_{S30} = 140$ –200 m/s, Amp. Factor = 7.0–7.99). These amplification factors are significantly higher than the NEHRP estimates. The difference between the NEHRP and our amplification factors likely results from different (i) levels of nonlinearity of site amplification, (ii) period, (iii) magnitude and distance range selected, and (iv) other details (Stewart and Seyhan 2013). The varying levels of nonlinearity in amplification factors derived from the use of different modulus reduction and damping (MRD) curves reflect epistemic uncertainty. This means that the knowledge on which set of MRD curves will yield the most correct ground response is lacking. Huang et al. (2010) have also reported

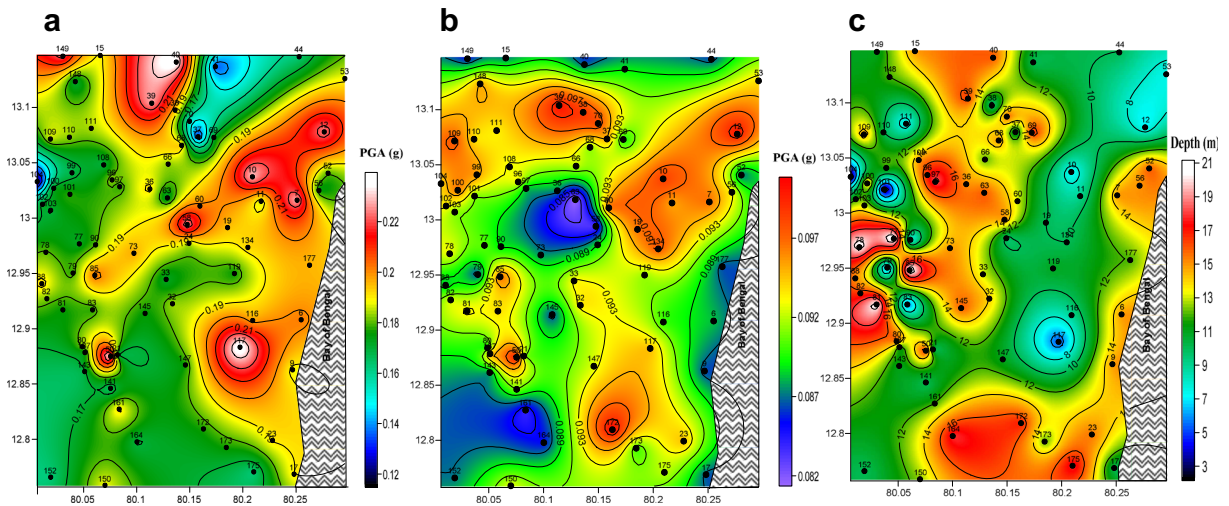


Fig. 8 Distribution of PGA at surface and rock level for the M6 target event in the city. **a** PGA distribution at surface level. **b** PGA distribution of depth of bedrock. **c** Distribution of depth to bedrock. Site locations are marked with a small circle and site numbers

with numerals shown on the map. Note that the northeastern part of the city is characterized by high PGA values both on the surface and rock

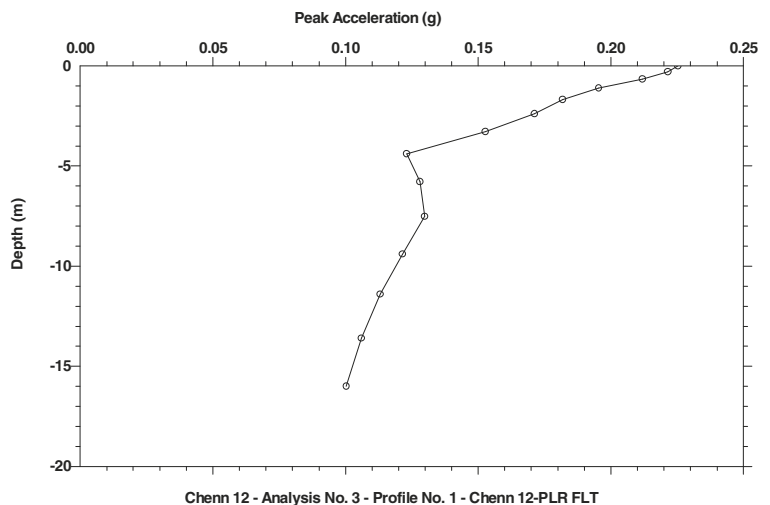
discrepancies between their and the NEHRP-derived site factors and have discussed in detail their probable causes. The above results suggest that high values of ground motion amplification and hence high PGA values are found for the parts of the city, where the shear wave velocity V_{S30} is low, representing areas of high seismic potential and hence high seismic hazard. Such a correlation between PGA and V_{S30} may always be not plausible, however, due to soil nonlinearity. Very soft sites sometimes deamplify at large shaking due to high damping at large shear strains.

4.1 Liquefaction potential in the Chennai city

As already mentioned, liquefaction potential can be characterized in terms of FS. If the value of the FS is in the range 1–2, then liquefaction potential is moderately severe. On the other hand, if its value is in the range > 2–3, then liquefaction potential is expected to be minimum (Sitharam et al. 2005).

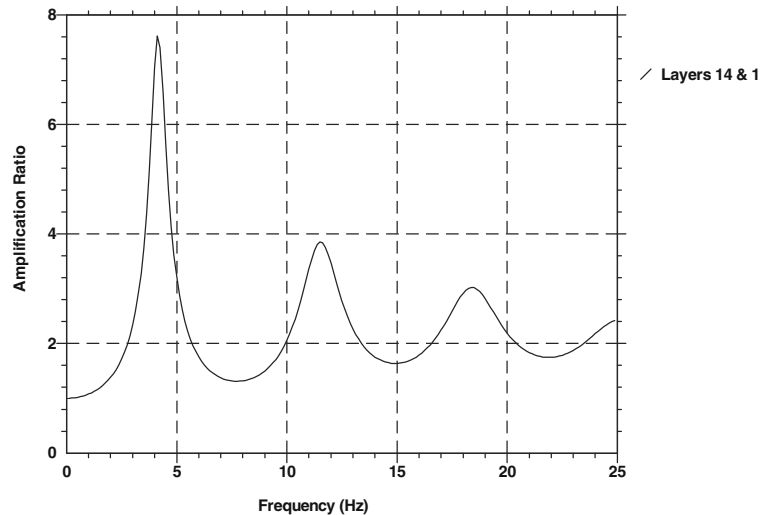
Figure 14 shows the map of the FS defined at surface level (Fig. 14a) and at 8-m depth (Fig. 14b) in the city. Because a major portion of the city has

Fig. 9 Variation of PGA with depth at site number no. 12 located in the northern part of the city for the M6 target event in the city. Note the relatively high value of PGA (> 0.1 g) at shallow depth (< 10 m)



Chenn 12 - Analysis No. 3 - Profile No. 1 - Chenn 12-PLR FLT

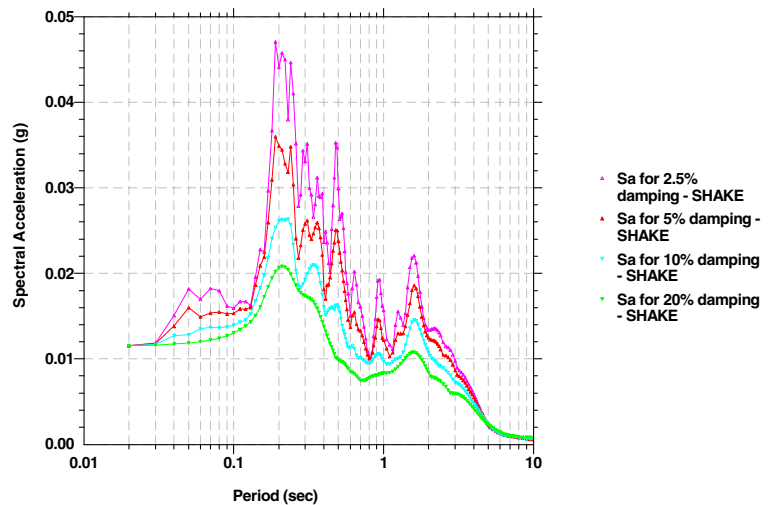
Fig. 10 Amplification ratio spectra between layers 14 (defined at 16-m depth) and 1 (defined at 0.145-m depth) for the site no. 12 located in the northern part of the city for the M6 target event in the city. Note the maximum amplification ratio around 4 Hz



the water table depth in the range 1–2 m (Ganapathy 2011), with the water table being rarely at the soil surface, one can rather evaluate liquefaction in this depth range. The difference in the FS value between these two cases is not expected to differ significantly, however. Liquefaction analyses carried out at 212 sites indicate that the values of FS, both at the surface and depth, are less than one at few sites (no. 12, no. 37, and no. 70) in the northern part of the city (Fig. 14). The values of FS for these three sites, when correlated with the gross geology of the area shown in Fig. 1, correspond to shear wave velocity of

less than 200 m/s with loose sand up to the 10–15-m depth and high PGA values. The northeast part along with few sites in southeast part of the city is characterized by relatively low FS values (< 1) than the remaining parts of the city. Thus, the northern part of the city seems to be more prone to liquefaction; our interpretation is mainly based on the values of the FS obtained, although one needs to consider additional information like exact composition of soil, their ability to liquefy, height of water table, etc. to further constrain liquefaction. Because these additional pieces of information are not available and our results are

Fig. 11 The response spectra at different damping levels at the ground surface at site number no. 12 for the M6 target event in the city. Note the maximum spectral acceleration around 0.2 s



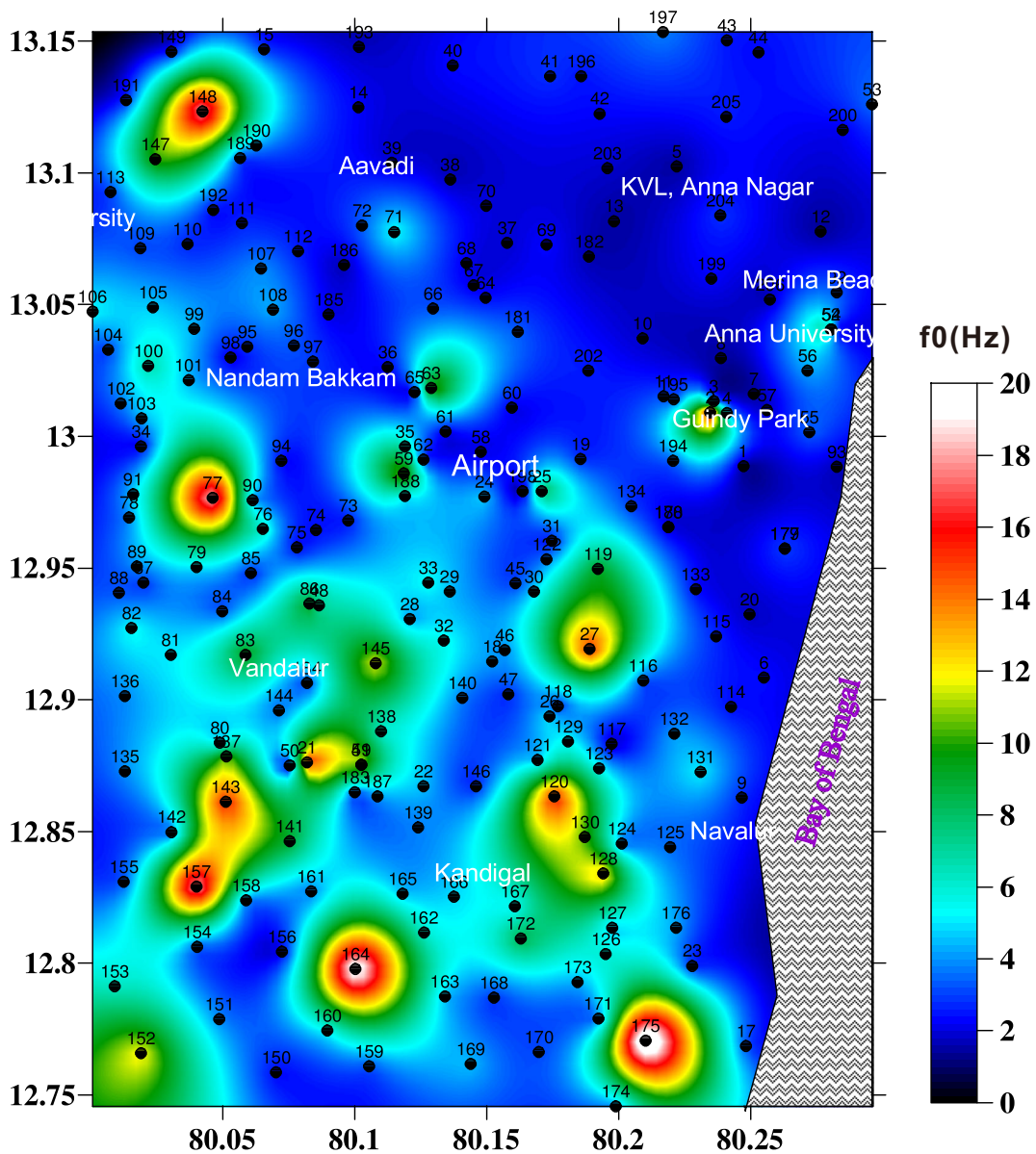


Fig. 12 Map of fundamental natural frequency for different sites in the city obtained for the M6 target event. Note the high values of fundamental frequency for sites scattered in the south-central to southern part of the city

based on the values of the FS only, hence the results obtained in this study can be considered as correct to the first order.

5 Conclusions

We study the spatial variation in ground motion parameters (PGA, site-specific response spectra), average shear wave velocity of upper 30-m soil column (V_{S30}),

amplification spectra, and factor of safety against liquefaction in the Chennai city, India. The results of this study are based on synthetic strong ground motion records calculated with the stochastic finite-fault modeling technique and site-specific response spectra calculated with one-dimensional ground response analysis at 210 sites in the city. The one-dimensional equivalent linear site response analysis is used to characterize the sites using the V_{S30} values obtained from the MASW survey. Average shear wave velocity V_{S30} at 5-m

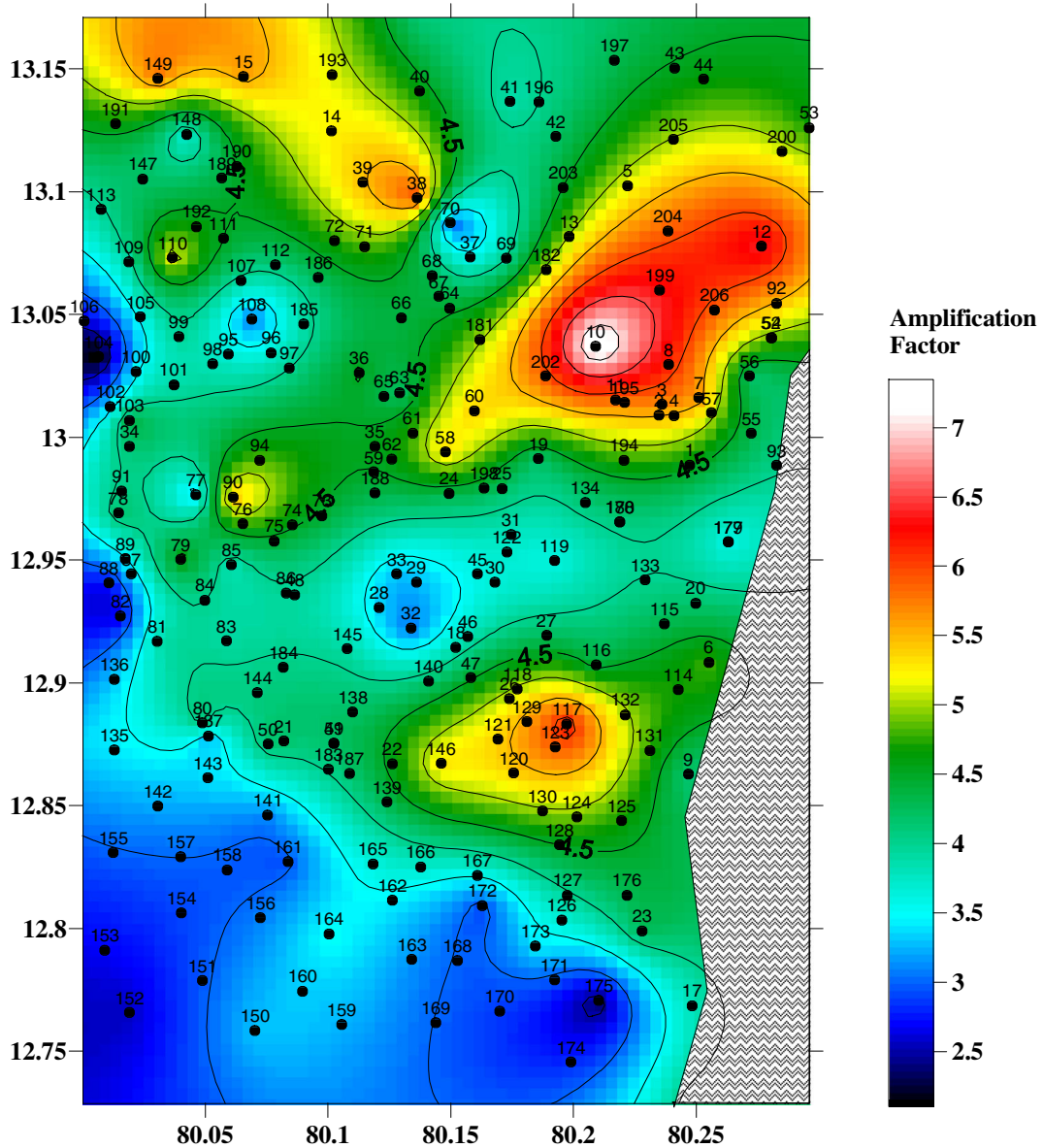


Fig. 13 Map of amplification factor for different sites in the city obtained for the target event M6. Note the high values of amplification ratio for the northeastern part of the city and few sites in the southern part like site no. 117 and no. 123

Table 4 Amplification factor and average V_{S30} values for different zones in the region

Zone	Amplification factor	Average V_{S30} (m/s)
I	3.0–3.99	750–1500
II	4.0–4.99	450–750
III	5.0–5.99	350–450
IV	6.0–6.99	200–350
V	7.0–7.99	140–200

interval up to a depth of 30 m is evaluated. The PGA values range from 0.11 to 0.24 g at surface and 0.08 to 0.13 g at rock site. A maximum PGA of 0.24 g observed at surface is probably associated with the presence of soft river basin alluvial deposits composed of silty clay/loose sandy silts and thus represents the effect of local soil condition on ground motion. The site-specific response spectra calculated for different damping levels show maximum amplification around 0.2 s. Liquefaction hazard map has been

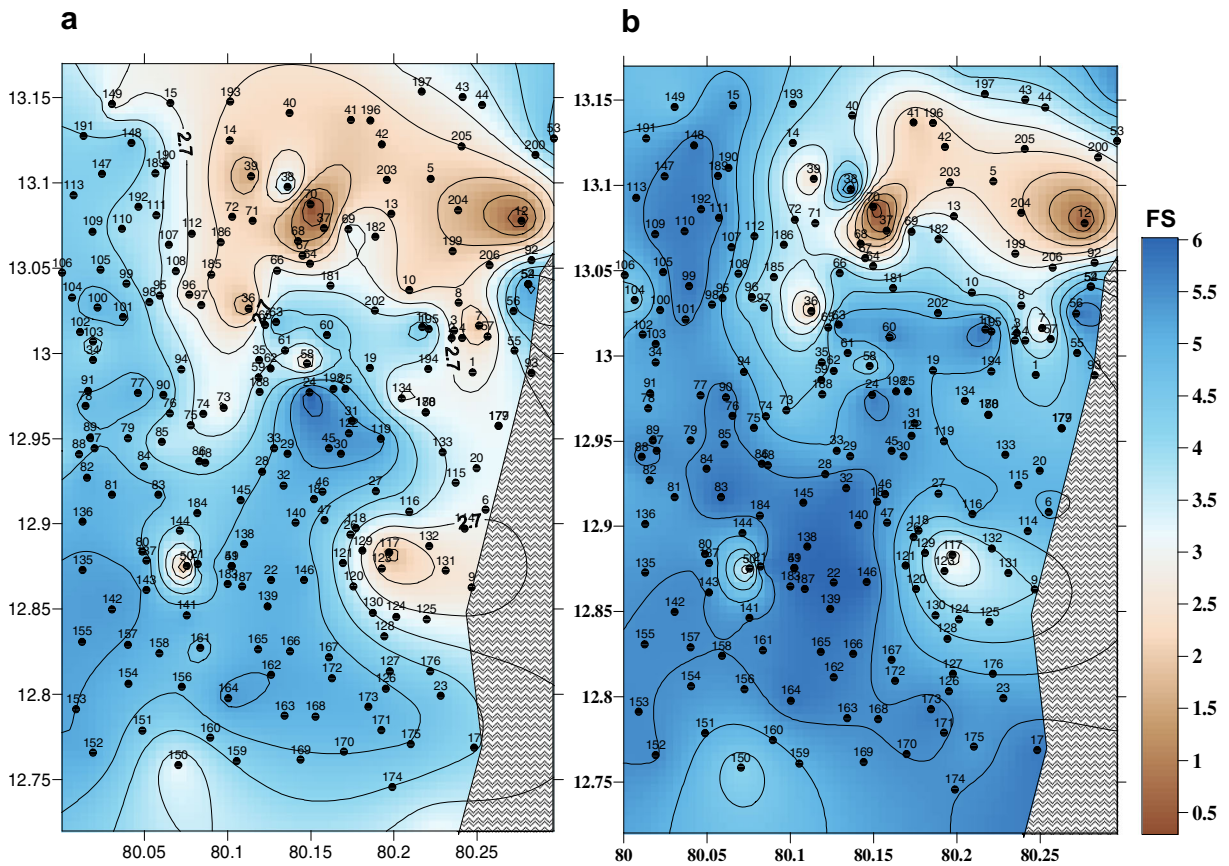


Fig. 14 Factor of safety (FS) against liquefaction over the city at **a** surface level and **b** at 8-m depth obtained for the M6 target event. Note the low values of FS both at the surface and at depth for few sites (no. 12, no. 37 and no. 70) in the northern part of the city

generated using the factor of safety against liquefaction. The results of this analysis show that the city is safe against liquefaction except at few locations where the overburden is alluvium with the presence of shallow water table.

The properties of earthquake source, the propagation characteristics of seismic waves through the earth to the top of bedrock, and characteristics of different sites in the city including the nonlinear soil response are helpful for obtaining a microzonation map, indicating the vulnerability of the area to potential seismic hazard. The map obtained here is based on only one magnitude of target event on the chosen source fault; hence, the estimates of PGA and the liquefaction potential may be underestimated and can be considered as correct to a first order. For obtaining more reliable estimates of these parameters, we need to analyze events of varying magnitude corresponding to different

source faults, as a scope of future study. In any case, the findings of this study will provide constraints to strengthen the built environment in the region to resist the effects of future earthquakes of similar magnitude and therefore to considerably reduce the expected losses. Thus, such information will be quite important in seismic hazard estimation, microzonation, and disaster management programs in the city.

Acknowledgements We sincerely thank the anonymous reviewer and the Editor Professor Kuvvet Atakan for their constructive comments that cleared several issues during revision. The author (NS) acknowledges the Council of Scientific and Industrial Research (CSIR) for providing the CSIR-RA Fellowship. NS thanks Drs. R. K. Tiwari, H. V. S. Satyanarayana, D. Srinagesh, and M. Kousalya for their encouragement. Director of CSIR-NGRI is thanked for his kind permission to publish this work. Some of the figures were produced using the Generic Mapping Tools software (Wessel and Smith 1995).

References

- Anbazhagan P, Sitharam TG (2008) Mapping of average shear wave velocity for Bangalore region: a case study. *J Environ Eng Geophys* 13(2):69–84
- Anderson J, Hough S (1984) A model for the shape of the Fourier amplitude spectrum of acceleration at high frequencies. *Bull Seismol Soc Am* 74:1969–1993
- Andrus RD, Stokoe KH II (2000) Liquefaction resistance of soils from shear-wave velocity. *J Geotech Geoenviron Engrg ASCE* 126(11):1015–1025
- Atkinson GM, Boore DM (1995) New ground motion relations for eastern North America. *Bull Seism Soc Am* 85:17–30
- Atkinson GM, Boore DM (2006) Earthquake ground-motion prediction equations for eastern North America. *Bull Seism Soc Am* 96(6):2181–2205
- Belloti R, Jamiolkowski M, Lo Presti DCF, O’Neill DA (1996) Anisotropy of small strain stiffness of Ticino sand. *Geotechnique* 46(1):115–131
- BIS: 1893 (2001) Indian standard, criteria for earthquake resistant design of structures. Bureau of Indian Standards, New Delhi
- Bodin P, Malagnini L, Akinci A (2004) Ground-motion scaling in the Kachchh basin, India, deduced from aftershocks of the 2001 Mw 7.6 Bhuj earthquake. *Bull Seism Soc Am* 94(5):1658–1669
- Boominathan A, Dodagoudar GR, Suganthi A, Uma Maheswari R (2008) Seismic hazard assessment of Chennai city considering local site effects. *J Earth Syst Sci* 117(S2):853–863
- Boore DM (1983) Stochastic simulation of high-frequency ground motions based on seismological models of the radiated spectra. *Bull Seismol Soc Am* 73:1865–1894
- Brune JN (1970) Tectonic stress and spectra of seismic shear waves from earthquakes. *J Geophys Res* 75:4997–5009
- Carlton BD, Tokimatsu K (2016) Comparison of equivalent linear and nonlinear site response analysis results and model to estimate maximum shear strain. *Earthquake Spectra* 32(3):1867–1887
- Di Bona M, Rovelli A (1988) Effects of the bandwidth limitation on stress drops estimated from integral of the ground motion. *Bull Seismol Soc Am* 78:1818–1825
- Dobry R, Iai S (2001) Recent developments in the understanding of earthquake site response and associated seismic code implementation. *Earthq Eng GeoEng2000 Conference Melbourne, Australia, November 2000*
- Ganapathy GP (2005) Seismic hazard assessment for Tamil Nadu state and a specific study on local ground motion response for part of Chennai city, India. Anna University, PhD thesis, 2005, p. 167 (Unpublished)
- Ganapathy GP (2011) First level seismic microzonation map of Chennai city—a GIS approach. *Nat Hazards Earth Syst Sci* 11:549–559
- Ganapathy GP, Rajawat AS (2014) Quantification of geologic hazard and vulnerability for Chennai city, India. *Int J Geomatics Geosci* 5(1)
- Goda K, Atkinson GM, Hunter AJ, Crow H, Motazedian D (2011) Probabilistic liquefaction hazard analysis for four Canadian cities. *Bull Seismol Soc Am* 101(1):190–201
- Hardin BO, Drnevich VP (1972) Shear modulus and damping in soils: design equation and curves. *J Soil Mechanics and Foundation, Division, ASCE, Vol. 98: SM7.667–692*
- Hashash YMA, Groholski DR, Phillips CA, Park D, Musgrove M (2011) DEEPSOIL 5.0, user manual and tutorial. University of Illinois at Urbana-Champaign, Champaign, p 107
- Huang YN, Whittaker AS, Luco N (2010) NEHRP site amplification factors and the NGA relationships. *Earthquake Spectra* 26:583–593
- Idriss IM (1999) An update to the Seed-Idriss simplified procedure for evaluating liquefaction potential. In: *Proceedings TRB workshop on new approaches to liquefaction*. January, Publication No. FHWA-RD-99-165, Federal Highway Administration
- Idriss IM, Boulanger RW (2006) Semi-empirical procedures for evaluating liquefaction potential during earthquakes. *Soil Dyn Earthq Eng* 26:115–130
- Idriss IM, Seed HB (1968) Seismic response of horizontal soil layers. *Proc ASCE J Soil Mech Found Eng* 94:1003–1031
- Imai T, Yoshimura Y (1970) Elastic wave velocity and soil properties in soft soil. *Tsuchi-to-Kiso* 18(1):17–22
- Iyengar RN, Ragukanth STG (2004) Attenuation strong ground motion in Peninsular India. *Seismol Res Lett* 75(4):530–540
- Kaklamanos J, Baise LG, Thompson EM, Dorfmann L (2015) Comparison of 1D linear, equivalent-linear, and nonlinear site response models at six KiK-net validation sites. *Soil Dyn Earthq Eng* 69:207–219
- Lee MKW, Finn WDL (1978) DESRA-2: dynamic effective stress response analysis of soil deposit with energy transmitting boundary including assessment of liquefaction potential, soil mechanics series. University of British Columbia, Vancouver
- Maheswari UR, Boominathan A, Dodagoudar GR (2010) Use of surface waves in statistical correlations of shear wave velocity and penetration resistance of Chennai soils. *Geotech Geol Eng* 28:119–137
- Matasovic N (1993) Seismic response of composite horizontally-layered soil deposits. Ph.D. Thesis, University of California, Los Angeles, CA
- Motazedian D, Atkinson GM (2005) Stochastic finite fault modeling based on a dynamic corner frequency. *Bull Seismol Soc Am* 95:995–1010
- Ohba Y, Goto N (1978) Empirical shear wave velocity equations in terms of characteristics soil indexes. *Earthq Eng Struct Dyn* 6:167–187
- Ordóñez GA (2003) SHAKE2000: a computer program for the 1-D analysis of geotechnical earthquake engineering problem. User’s manual. <http://www.shake2000.com/>
- Padhy S, Subhadra N (2016) Spectral scaling and seismic efficiency for earthquakes in Northeast India. *Bull Seismol Soc Am* 106(4):1613–1627
- Park CB, Miller RD, Xia J (1999a) Multichannel analysis of surface waves (MASW). *Geophysics* 64:800–808
- Park CB, Miller RD, Xia J (1999b) Multimodal analysis of high frequency surface waves. In: *Proceedings of the symposium on the application of geophysics to engineering and environmental problems (SAGEEP 90)* Oakland. 115–122
- Radhakrishna BP (1992) Cauvery—its geological past. *J Geol Soc India* 40(1):1–12
- Rao JU, Babu VRRM (1995) A quantitative morphometric analysis of Gundala Kamma River basin, Andhra Pradesh. *Ind J Earth Sci* 22:63–74
- Robertson PK, Woeller DJ, Finn WDL (1992) Seismic cone penetration test for evaluating liquefaction potential under cyclic loading. *Can Geotech J* 29:686–695

- Roesler S (1979) Anisotropic shear modulus due to stress anisotropy. *J Geotechnical Eng Division, ASCE*, 105, GT7: 871–880
- Schnabel PB (1973) Effects of local geology and distance from source on earthquake ground motion. Ph.D. Thesis, University of California, Berkeley
- Seed HB, Idriss IM (1970) Soil moduli and damping factors for dynamic response analysis. Report no. EERC 70-10. University of California, Berkeley
- Seed HB, Idriss IM (1971) Simplified procedure for evaluating soil liquefaction potential. *J Soil Mech Found Div ASCE* 97(9):1249–1273
- Seed HB, Wong RT, Idriss IM, Tokimatsu K (1986) Moduli and damping factors for dynamic analyses of cohesionless soils. *J Geotech Eng ASCE* 112(11):1016–1032
- Singh SK, Garcia D, Pacheco JF, Valenzuela R, Bansal BK, Dattatrayam RS (2004) Q of the Indian shield. *Bull Seismol Soc Am* 94:1564–1570
- Sitharam TG, Anbazhagan P, Mahesh GU, Bharathi K, Reddy NP (2005) Seismic hazard studies using geotechnical borehole data and GIS. Proc Symp on Seismic Hazard Analysis and Microzonation. Sep. 2005, Roorkee
- Stewart JP, Seyhan E (2013) Semi-empirical nonlinear site amplification and its application in NEHRP site factors. PEER Report 2013/13 Pacific Earthquake Engineering Research Center College of Engineering University of California, Berkeley, November 2013: 13–22
- Stokoe KH, Nazarian S (1985) Use of Rayleigh waves in liquefaction studies proceedings, measurement and use of shear wave velocity for evaluating dynamic soil properties. *J Geotech Eng Div ASCE*, May, 1–17
- Subhadra N, Padhy S, Prasad PP, Seshunarayana T (2015) Site specific ground motion simulation and seismic response analysis for microzonation of Nanded city, India. *Nat Hazards* 78:1749–1938. <https://doi.org/10.1007/s11069-015-1749-z>
- Sun JI, Golesorkhi R, Seed HB (1988) Dynamic moduli and damping ratios for cohesive soils. Report No. EERC 88-15, University of California, Berkeley
- Wells DL, Coppersmith KJ (1994) New empirical relationships among magnitude, rupture length, rupture width, rupture area, and surface displacement. *Bull Seismol Soc Am* 84: 974–1002
- Wessel P, Smith WHF (1995) New versions of the generic mapping tools released. *EOS Trans AGU* 76:329
- Youd TL, Idriss IM, Andrus RD, Arango I, Castro G, Christian JT, Dobry R, Finn WDL, Harder Jr.LF, Hynes ME, Ishihara K, Koester JP, Liao SSC, Marcuson III WF, Martin GR, Mitchell JK, Moriwaki Y, Power MS, Robertson PK, Seed RB, Stokoe II, KH (2001) Liquefaction resistance of soils summary report from 1996 NCEER and 1998 NCEER/NSF workshops on evaluation of liquefaction resistance of soil. *J Geotech Geoenviron Eng* 127: 817–833
- Zhao JX (2011) Comparison between V_{S30} and site period as site parameters in ground-motion prediction equations for response spectra, 4th IASPEI/IAEE International Symposium, University of California Santa Barbara